On shear-banding and wormlike micellar system response under complex flow

J. Esteban López-Aguilar[1], Michael F. Webster[1], Hamid R. Tamaddon-Jahromi[1], and Octavio Manero[2]

[1] Institute of Non-Newtonian Fluid Mechanics, Swansea University, College of Engineering, Bay Campus, Fabian Way, Swansea, SA1 8EN, UK
[2] Instituto de Investigaciones en Materiales, UNAM, 04510, Mexico.

ABSTRACT

This study focuses on *fv/fe* modelling of *shear-banded* wormlike micellar fluids in complex flow using a *revised BMP+_*τ_p *model*. A *modified planar Couette-flow* is generated by a moving-top-plate over a rounded-corner 4:1:4 planar contraction-expansion. Pure-shear Couette-flow is observed in fully-developed entry-exit regions, whilst mixed shear-extensional flow arises around the contraction-zone.

INTRODUCTION

The theme of this predictive modelling study is particularly concerned with investigating material systems, of worm-like micellar form, that are capable of supporting shear-banded flow response. Typically, under ideal shear-flow, but developing this further, to identify the corresponding position adopted under complex flow scenarios. There is sparsity of evidence in the literature for complex flow, in segregating such shear-banded material response. For this purpose, a *revised BMP+_*τ_p *model* is introduced to represent the response of wormlike micellar systems under shear-banding conditions. New and preferential features to this advanced BMP+_τ_p model-variant (Lopez-Aguilar et al[1,2]) are bounded extensional-viscosity response and an N_{1Shear}-upturn at high deformation-rates. The majority of background work on this topic has been performed largely whilst focussing on steady simple-shear flow, and is commonly restricted to Couette-flow deformation (see Divoux et al.[3]). Experimental evidence would indicate that, extremely polymer-concentrated micellar-fluids, with non-monotonic shear-stress, are required to generate shear-banded solutions. As such, banded-system response is sought under solvent-fractions of $\beta \leq 10^{-2}$ and material shear-banding intensity parameters of $\xi \gtrsim 3$ (with $\xi=0$, representing non-banding systems).

GOVERNING EQUATIONS & THEORETICAL FRAMEWORK

According to experiments (Divoux et al.[3], García-Sandoval et al.[4]) and conventional simple-shear flow modelling, to promote exposure to shear-banding, a combination of factors are necessary. Firstly, a deformation-rate that is dependent on the destruction coefficient; and secondly, extremely polymer-concentrated fluids, with solvent-fractions on the order of $\beta \leq 10^{-2}$. With the BMP-family of fluids and in the structure-equation, non-monotonicity is introduced through an explicit rate-dependence on the structure destruction coefficient. Such dependency is expressed in Eq.(1), as a linear function of the destruction-coefficient, whilst also calling upon the second-invariant on the rate-of-deformation tensor II_D:

$$\left(\frac{\partial}{\partial t}+\boldsymbol{u}\cdot\nabla\right)f=\frac{1}{\omega}(1-f)+\left(1+\zeta II_{\boldsymbol{D}}\right)\left(\xi_{G_0}Wi-\xi f\right)\left|\boldsymbol{\tau}_p:\boldsymbol{D}\right| \qquad (1)$$

In this, a new temporal-scale arises, that of the shear-banding intensity parameter ($\zeta=\vartheta\frac{U}{L}$ in dimensionless form). This parameter then directly relates to flow-segregation. At sufficiently high polymer concentrations and against deformation-rate increase, the shear-banding intensity parameter ζ dictates - the appearance of maxima in the T_{rz}-flow-curve, and the intensity of the shear-stress T_{rz}-drop and subsequent rise. When ζ =0 (non-banding systems), a monotonic T_{rz}-flow-curve is recovered. In addition, the dimensionless micellar coefficients account for structural-construction ($\omega=\lambda_s\frac{U}{L}$, as a dimensionless time) and structural-destruction ($\xi_{G_0}=\frac{k_0G_0}{\eta_\infty+\delta}\left(\eta_{p0}+\eta_s\right)$ and $\xi=k_0\left(\eta_{p0}+\eta_s\right)\frac{U}{L}$). Note, in Eq.1, the explicit presence of the group Weissenberg number ($Wi=\lambda_1U/L$), which determines elastic response. Hence, the structure-equation (Eq.1) provides a dimensionless fluidity $f=\frac{\eta_{p0}}{\eta_p}$ with a coupled highly-nonlinear relationship established amongst structure dynamics, viscoelasticity and energy-dissipation. Such a dimensionless fluidity f supplies information on both, the internal structure of the fluid, and modulates the polymeric-stress $\boldsymbol{\tau}_p$-contribution; itself governed by:

$$Wi\overset{\nabla}{\boldsymbol{\tau}}_p=2(1-\beta)\boldsymbol{D}-f\boldsymbol{\tau}_p. \qquad (2)$$

Here, the upper-convected derivative of polymeric-stress is,
$\overset{\nabla}{\boldsymbol{\tau}}_p=\frac{\partial\boldsymbol{\tau}_p}{\partial t}+\boldsymbol{u}\cdot\nabla\boldsymbol{\tau}_p-\nabla\boldsymbol{u}^T\cdot\boldsymbol{\tau}_p-\boldsymbol{\tau}_p\cdot\nabla\boldsymbol{u}$.
Eq.(1-2) together deliver the internal forces within the polymeric-component of these wormlike micellar fluids. These then combine with a complementary Newtonian-contribution, $\boldsymbol{\tau}_s=2\beta\boldsymbol{D}$, to generate the total extra-stress $\boldsymbol{T}=\boldsymbol{\tau}_s+\boldsymbol{\tau}_p$. Here, $\beta=\eta_s/\left(\eta_{p0}+\eta_s\right)$ represents a solvent-fraction, where η_s is the solvent-viscosity. The usual field equations apply for incompressible and isothermal flow, viz:

$$\nabla\cdot\boldsymbol{u}=0, \qquad (3)$$

$$Re\frac{\partial\boldsymbol{u}}{\partial t}=\nabla\cdot\boldsymbol{T}-Re\boldsymbol{u}\cdot\nabla\boldsymbol{u}-\nabla p, \qquad (4)$$

adopting a group Reynolds number, $Re=\rho UL/\left(\eta_{p0}+\eta_s\right)$, with material density, ρ (here, Re~O(10^{-2}).

Discretisation: To extract numerical solutions under such severe and highly non-linear flow conditions (recall β~10^{-2} and high *Q*-requirements), the *ABS-f* correction is demanded. This correction to the constitutive equation enhances numerical tractability, by enforcing consistent material property estimation. Continuity satisfaction is enforced discretely and a VGR-correction is also adopted (Lopez-Aguilar et al[1,2]).
The numerical method employed is one of a hybrid finite element/volume scheme[1,2]. This scheme is a semi-implicit, time-splitting, fractional three-staged formulation. It invokes finite element (*fe*) discretisation for velocity-pressure (Q2-Q1, parent-cell) discretisation and cell-vertex finite volume (*fv,* subcell) discretisation for stress. In this, the individual advantages and benefits of both (*fe*) and (*fv*) schemes are combined. The sub-cell *fv*-triangular-

tessellation is constructed within the parent *fe*-grid by connecting the mid-side nodes. In such a structured tessellation, stress variables are located at vertices of *fv*-sub-cells, offering linear interpolation whilst circumventing solution projection. The sub-cell, cell-vertex *fv*-scheme is constructed about - fluctuation-distribution techniques for advection terms (upwinding), and median-dual-cell treatment for additional source terms (inhomogeneity)[3,4].

RESULTS & DISCUSSION

The flow curve – steady simple shear flow

Flow-curves for a segregating and a non-segregating fluids are plotted in Fig. 1a. Here, shear stress T_{rz} against shear-rate data display two different behavioural responses: 1) for a non-segregating fluid, with shear-banding parameter ζ=0; and 2) for a segregating fluid, with ζ=3 (which provokes a maximum in the flow-curve). Such fluids have an extremely low solvent-fraction of β=10^{-2}, as well as moderate-hardening extensional features $\{\omega, \xi_{G0}, \xi, \delta\}$={4, 0.1136, 2.27x$10^{-5}$, 1x$10^{-6}$}, see López-Aguilar et al.[3,4].

Complex flow - Modified Couette flow

A choice of three overall deformation-rates $\lambda_1\dot{\gamma}_0$ have been selected to explore segregating and non-segregating flow regimes, as in Fig. 1 flow-curve. Here, and via the drag exerted by the moving top-plate, low ($\lambda_1\dot{\gamma}_0$=0.5, Q=4), intermediate ($\lambda_1\dot{\gamma}_0$=3.75, Q=30), and high ($\lambda_1\dot{\gamma}_0$=56, Q=450) overall shear-rates $\dot{\gamma}_0$ (=U_{wall}/L) are imposed. Flow profiles for these overall shear-rates are tested on two fluids: Fluid-I, incapable of supporting flow-segregation (with null shear-banding intensity parameter; ζ=0); and Fluid-II, prone to generate shear-banding (ζ=3). This (ζ=3)-Fluid-II may manifest shear-bands in an intermediate shear-rate interval of $1 \le \lambda_1\dot{\gamma}_0 \le 10$. The stated combination, of three overall shear-rates and two fluids, provides six instances to compare and contrast (listed in Table 1). Here, attention is restricted to, contrasting case-E banded solutions (Fluid-II), against counterpart case-B non-banded (Fluid-I) instances; and also case-D, with the segregating Fluid-II in the non-banding flow-rate situation.

Table 1. Deformation-rate versus fluid chart

	$\lambda_1\dot{\gamma}$=0.5 Q=4	$\lambda_1\dot{\gamma}$=3.75 Q=30	$\lambda_1\dot{\gamma}$=56.25 Q=450
ζ=0 non-segregating Fluid-I	A Non-banded	B Non-banded	C Non-banded
ζ=3 segregating Fluid-II	D Non-banded	E *Banded*	F Non-banded

Banded against Non-banded solutions – Intermediate flow rate ($\lambda_1\dot{\gamma}$=3.75), E v B cases

E-Banded velocity-u_x field and profile First, the ζ=3-banded *D*-case is considered (Table 1), for which the corresponding velocity u_x-field is presented in Fig. 2a. The nature of this complex planar flow, reveals simple shear-flow away from the contraction, and a combined shear-extensional deformation in the contraction-region. In the upstream and downstream *fully-developed flow-regions*, one may appreciate a non-homogeneous steady-state velocity u_x-field, with velocity-bands exposed in the vertical *y*-spatial direction. Such a segregated flow pattern is then lost in the approach to the constriction. Subsequently, one notes that, after traversing through the constriction and upon recovering simple-shear deformation, a fully-developed flow pattern is recovered (as upstream).

In Fig. 3a, flow-segregation is recorded through a split u_x-profile. The interface between bands is located at the inflectionpoint of such a split u_x-profile (y_{int}~3.48 units), where a sharp-change of colour-intensity in the fields may be gathered (Fig. 2). The location of this interface is determined at: $y_{int} = \frac{\dot{\gamma}_2 - \dot{\gamma}_0}{\dot{\gamma}_2 - \dot{\gamma}_1}\alpha_d$, where $\dot{\gamma}_0$ (=3.8 units and T_{rz}~0.4; Fig.1) is the overall shear-rate (here, in the unstable shear-stress regime). Then, at an equivalent shear-stress level, $\dot{\gamma}_1$ (=0.6 units) and $\dot{\gamma}_2$ (=25 units) are the low and high shear-rate stable-branches, respectively. In addition, α_d=4 units, is the distance that separates the moving-plate and the contraction wall, corresponding to the contraction ratio (α) in this instance. Each velocity-band is supported by the corresponding low-$\dot{\gamma}_1$ and high-$\dot{\gamma}_2$ shear-rates. The narrow band in the local neighbourhood of the moving-plate (Fig. 2a), corresponds to the material in the high-$\dot{\gamma}_2$ shear-rate band. In terms of rheological response (Fig. 1), this high-$\dot{\gamma}_2$ shear-rate band corresponds to a highly-unstructured fluid of total-viscosity η_{Tot}~1.8x10^{-2} units. In contrast, the low-$\dot{\gamma}_1$ shear-rate band occupies the remaining channel space, lying between the band-interface and the bottom geometry-wall (Fig. 2a). Here, a highly-structured fluid is reported, with viscosity η_{Tot}~0.8 units. In the *complex flow region*, the pre-banded flow field is disrupted and distorted by the constriction, with unstructured material flowing through the constriction-gap, and highly-structured material occupying the stagnant corners (see the viscosity field representation, Fig. 2b). Then, beyond the constriction, and once the fluid-viscosity has had opportunity to readjust, a banded morphology is reformed.

Shear and normal stress fields The fully-developed banded velocity profile response of ζ=3-solution, is accompanied by a roughly constant shear-stress T_{rz}-field (Fig. 2c). Notably, at the channel-height where the interface between bands appears, a horizontal stripe of slightly larger T_{rz}-values is apparent. The counterpart T_{rz}-profile (Fig. 3b) reveals a constant T_{rz}-level (~0.4 units), that appears throughout the flow-gap. Nevertheless, precisely near the interface location, the T_{rz}-profile oscillates; such undulation coincides with the slightly more intense stripes observed, and may be associated with the discontinuity posed by the interface. Conspicuously, the normal-stress T_{xx} also inherits bands, driven by the velocity profile (Fig. 2d). Once more, the homogeneous T_{rz}-field and the inhomogeneous T_{xx}-response in the fully-developed regions, are disturbed by the presence of the constriction. Here, the effects of the combined shear-extensional deformation are more evident. On T_{rz}, the stripped-interface disappears and a homogeneous T_{rz}-level is adopted in the constriction-gap; moreover, in the recess-zones, there are triangular structures, and a localised small zone emerges on the contraction back-face, near its tip. Consistently, on T_{xx}, two regions are reported; with base on the contraction-tip, of negative values upstream, and a positive counterpart downstream.

B-Non-banded Velocity field For case-*B* (non-segregating fluid (ζ=0): Table 1) and taken in contrast to case-*E* (ζ=3), the fully-developed velocity u_x-field now appears in single and continuous shear-rate form. This is accompanied by upstream/downstream constant T_{rz}- and T_{xx}-levels. Such a linear upstream velocity-profile is lost in the constriction zone, where the fluid is accelerated as a consequence of the converging flow. Here, given the highly-nonlinear conditions based on polymer-content (β=10^{-2}) and increased flow-rate, the pressure-drop to drive the flow is enforced through a fixed pressure boundary condition at the inlet. This implies that the resulting pressure level must be calculated at the flow-outlet. Such a procedure ensures that there is no downstream blockage created in pressure. Otherwise, this may arise to degrade the downstream solution quality in taking up fully-developed flow conditions.

CONCLUSIONS

In this study, novel solutions are reported on shear-banding flow of micellar systems in complex flow scenarios. Based on two micellar fluids with segregating and non-segregating features, solutions display banded and non-banded structures away from the constriction, respectively. In the banded-case, such segregation is disrupted upon the approach to the contraction region in complex flow; and yet, is rebuilt, once the constriction has been traversed and the material returned to steady shear-flow. Such spontaneous segregation in the fully developed regions away from the contraction is supported by distinctly low and high deformation rates, which accordingly provide bands in velocity, normal stresses and viscosity (fluid structure). In contrast, non-segregating fluids display homogeneous fields at equivalent flow-rates.

REFERENCES

1. López-Aguilar, J.E., Webster, M.F., Tamaddon-Jahromi, H.R., and Manero O. (2016) "A comparative numerical study of time-dependent structured fluids in complex flows", *Rheol. Acta,* **55** 197–214.

2. López-Aguilar, J.E., Webster, M.F., Tamaddon-Jahromi, H.R., and Manero O. (2016) "Convoluted models & high-Weissenberg predictions for micellar thixotropic fluids in contraction-expansion flows", *J. Non-Newtonian Fluid Mech.,* **232** 55–66.

3. Divoux, T., Fardin, M.A., Manneville, S., and Lerouge, S. (2016) "Shear banding of complex fluids", *Annu. Rev. Fluid Mech.,* **48** 81–103.

4. García-Sandoval J.P., Manero, O., Bautista, F., and Puig, J.E. (2012) "Inhomogeneous flows and shear-banding formation in micellar solutions: predictions of the BMP model", *J. Non-Newtonian Fluid Mech.,* **179-180** 43–54.

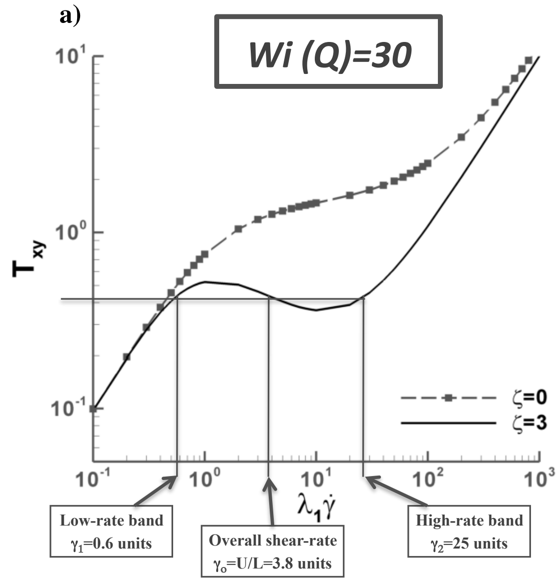

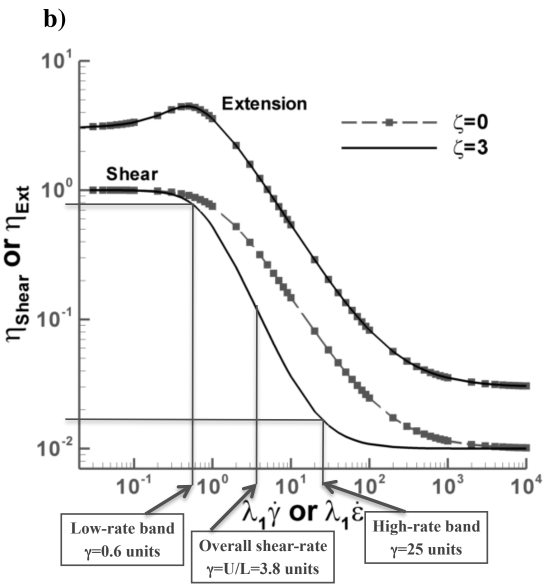

Figure 1. a) T_{xy} and b) viscosity; BMP+_τ_p MH; non-segregating ζ=0 and segregating ζ=3 fluids

a) $\boldsymbol{u_x}$

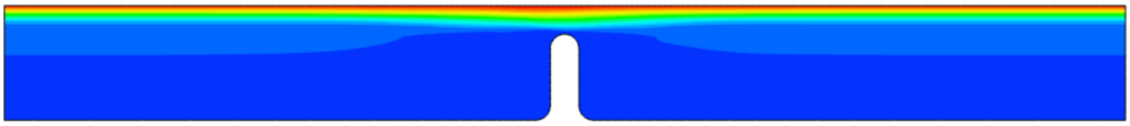

b) ***Viscosity***

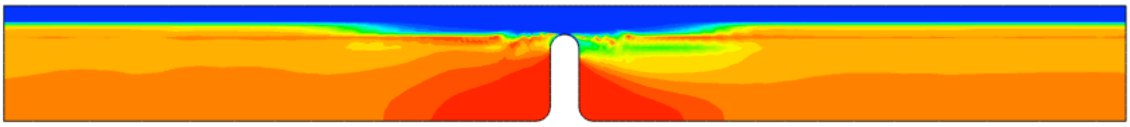

c) $\boldsymbol{T_{xy}}$

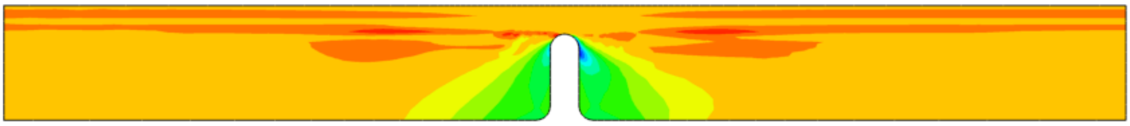

d) $\boldsymbol{T_{xx}}$

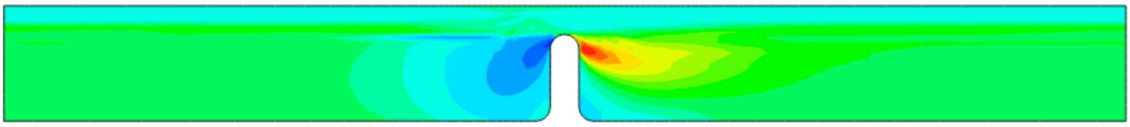

Figure 2. a) u_x, b) viscosity, c) T_{xy} and d) T_{xx}; BMP+_τ_p MH; Case E: {Q, ζ}={30, 3}

a
`

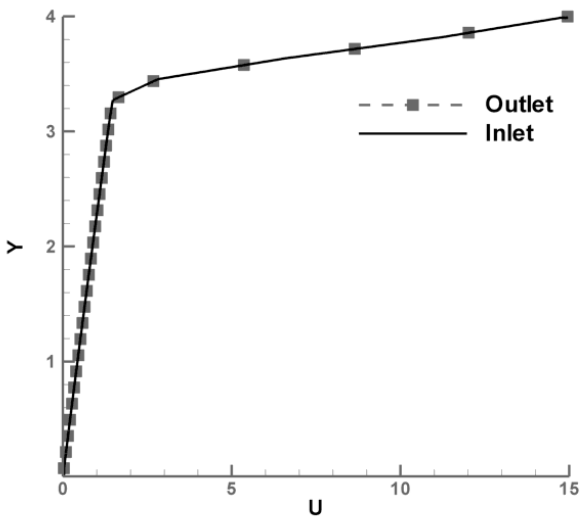

b)

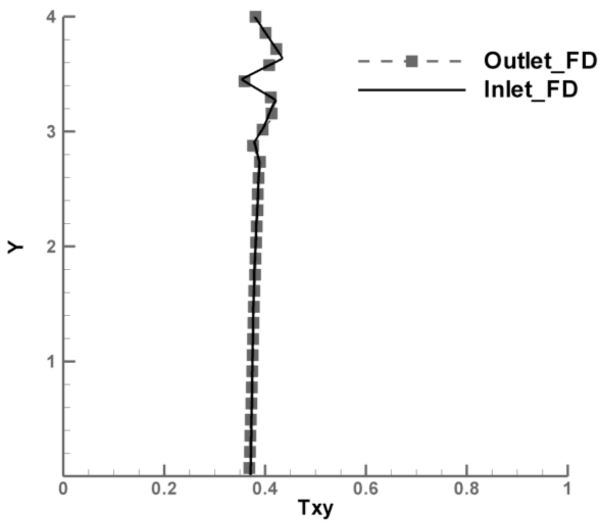

Figure 3. a) u_x and b) T_{xy} profiles; BMP+_τ_p MH; Case E: {Q, ζ}={30, 3}